CORONAVIRUS

Direct detection of human adenovirus or SARS-CoV-2 with ability to inform infectivity using DNA aptamer-nanopore sensors

Ana S. Peinetti[1†], Ryan J. Lake[1], Wen Cong[2], Laura Cooper[3], Yuting Wu[1], Yuan Ma[1], Gregory T. Pawel[1], María Eugenia Toimil-Molares[4]*, Christina Trautmann[4,5], Lijun Rong[3]*, Benito Mariñas[2]*, Omar Azzaroni[6]*, Yi Lu[1]*

Viral infections are a major global health issue, but no current method allows rapid, direct, and ultrasensitive quantification of intact viruses with the ability to inform infectivity, causing misdiagnoses and spread of the viruses. Here, we report a method for direct detection and differentiation of infectious from noninfectious human adenovirus and SARS-CoV-2, as well as from other virus types, without any sample pretreatment. DNA aptamers are selected from a DNA library to bind intact infectious, but not noninfectious, virus and then incorporated into a solid-state nanopore, which allows strong confinement of the virus to enhance sensitivity down to 1 pfu/ml for human adenovirus and 1×10^4 copies/ml for SARS-CoV-2. Applications of the aptamer-nanopore sensors in different types of water samples, saliva, and serum are demonstrated for both enveloped and nonenveloped viruses, making the sensor generally applicable for detecting these and other emerging viruses of environmental and public health concern.

INTRODUCTION

Viral infections are an important public health issue, as viral outbreaks, such as the recent coronavirus disease 2019 (COVID-19) pandemic, have resulted in enormous economic and societal impacts around the world. Critical to addressing this issue is timely and accurate viral diagnosis in both biological and environmental samples to enable the prompt treatment of viral infections while preventing the spread of viruses. It is thus important to develop a method that can rapidly detect virus particles at extremely low levels in complex samples (*1*) and without sample pretreatment to minimize false-negative and false-positive results. Of the widely used existing viral detection methods, viral nucleic acid detection using quantitative polymerase chain reaction (qPCR) has become the reference standard method due to its high sensitivity. However, this detection process requires long analysis time and expensive laboratory instruments, which limits its speed and availability. Other nucleic acid detection methods have been developed to address some of these issues to make tests based on genome detection more portable and accessible (*2*, *3*). However, they still generally require sample pretreatment to extract the viral RNA and equipment to control the temperature during amplification (*4*). Alternatively, serological tests that detect antibodies (*5*) or immuno-tests that detect antigens (*6*) have shown potential to provide results at faster speed and requiring less sample pretreatment. However, antibodies produced in patients can only be detected 1 to 2 weeks after disease onset as opposed to viral RNA, which can be detected within the first few days (*7*). Hence, serological tests are generally not suitable for viral disease diagnosis. In addition, direct antigen detection generally has lower specificity and sensitivity compared to the nucleic acid–based tests (*8*).

Most critically, none of the current COVID-19 tests are able to differentiate infectious from noninfectious viruses, because the detection of viral nucleic acids, patient antibodies, or antigens alone does not indicate that intact infectious virus is present and levels of these biomarkers have shown poor correlation with infectivity (*9*). For instance, it has been shown that the severe acute respiratory syndrome coronavirus 2 (SARS-CoV-2) viral RNA can remain detectable in some patients for more than 1 month after onset of illness, while viable virus could not be detected by culture after week 3 (*10*). In addition, viruses present in environmental samples, such as in air or water or on different surfaces, can also be a major route for spreading infection. However, tests that are based on detection of viral nucleic acids or proteins cannot determine whether the virus has been rendered noninfectious (inactivated) or is still infectious (active). The gold standard method for direct detection of viruses that can inform infectivity continues to be microbiology techniques, namely, plaque assays; however, it takes several days to grow plaques and requires growing the virus within host cells, which increases the required labor, expertise, and equipment and will not work for viruses that do not replicate well in cell culture systems (*11*). Therefore, despite many years of research and numerous publications, few existing methods can allow direct and ultrasensitive detection and quantification of intact viruses with the ability to

[1]Department of Chemistry, University of Illinois at Urbana-Champaign, Urbana, IL 61801, USA. [2]Department of Civil and Environmental Engineering, Safe Global Water Institute, University of Illinois at Urbana-Champaign, Urbana, IL 61801, USA. [3]Department of Microbiology and Immunology, College of Medicine, University of Illinois at Chicago, Chicago, IL 60612, USA. [4]GSI Helmholtzzentrum für Schwerionenforschung, Darmstadt 64291, Germany. [5]Technische Universitat Darmstadt, Darmstadt 64287, Germany. [6]Instituto de Investigaciones Fisicoquímicas Teóricas y Aplicadas (INIFTA), Departamento de Química, Facultad de Ciencias Exactas, Universidad Nacional de La Plata (UNLP), CONICET, Boulevard 113 y 64, La Plata 1900, Argentina.
*Corresponding author. Email: yi-lu@illinois.edu (Y.L.); azzaroni@inifta.unlp.edu.ar (O.A.); marinas@illinois.edu (B.M.); lijun@uic.edu (L.R.); m.e.toimilmolares@gsi.de (M.E.T.-M.)
†Present address: INQUIMAE (CONICET), Departamento de Química Inorgánica, Analítica y Química Física, Facultad de Ciencias Exactas y Naturales, Universidad de Buenos Aires, Ciudad Universitaria, Pabellón 2, C1428EHA, Buenos Aires, Argentina.

inform on infectivity. As a result, misdiagnoses and delayed treatment continue to occur daily and worldwide, especially given the fact that many asymptomatic people can transmit viruses unknowingly, which can result in further spread of viral disease.

To overcome the limitations of current methods, we here report an efficient method for direct detection of intact viruses without sample pretreatment, with the ability to differentiate infectious from noninfectious viruses and to reach low detection limits. Our method integrates a highly selective DNA aptamer with a highly sensitive solid-state nanopore to selectively detect infectious viruses in both biological and environmental samples. This aptamer-nanopore sensor has been demonstrated for both human adenovirus (HAdV), which is a nonenveloped double-stranded DNA (dsDNA) virus that is responsible for respiratory water-borne diseases that especially affect children worldwide (*12*), and also a SARS-CoV-2 pseudotyped virus that incorporates the spike (S) protein of SARS-CoV-2 into a lentivirus, which mimic the surface of the native SARS-CoV-2, the enveloped single-stranded RNA (ssRNA) coronavirus that is responsible for the current COVID-19 pandemic. The wide diversity in viruses that our sensor can detect, in terms of both viral genome and envelope type, demonstrates that our method is generally applicable to a wide range of current and future emerging viruses.

RESULTS

To assess the infectivity of a virus, a major challenge is finding a sensing molecule that can bind and selectively recognize intact infectious viruses and differentiate it from both the same virus that has been rendered noninfectious and also from other viruses. To meet this challenge, we used DNA aptamers as the recognition agent to selectively bind to an intact infectious virus. These DNA aptamers are DNA molecules with a specific sequence that allow them to form a specific 3D shape that can recognize a certain target with high affinity and selectivity that rivals antibodies and yet are less expensive and more stable (*13*). They can be obtained synthetically in a test tube using a combinatorial selection technique called systematic evolution of ligands by exponential enrichment (SELEX) or in vitro selection, in which sequences with high affinity are enriched from a DNA library of 10^{15} random sequences. Multiple selection rounds can be performed to gradually enrich the pool, with PCR amplification used in between rounds to restore the amount of DNA before each subsequent round. In addition, the conditions for SELEX can be tailor-made to remove competing targets from known interfering species using counterselection (*14*). For the first selection target, HAdV, we designed the SELEX to include both positive selection steps to retain any DNA molecules that bind to infectious HAdV and counterselection steps to discard any DNA sequences that bind to the same HAdV that had been rendered noninfectious by free chlorine treatment (*15*). A schematic representation of the selection process is shown in Fig. 1A, and details of the positive and counterselections are given in Materials and Methods and Table 1. In addition, SELEX was performed using the whole virus as the target, instead of a specific biomarker for the virus, such as a viral surface protein. In doing so, we aimed to select aptamers that will bind to the target in its native state, without the need for disruption of the virus (*16*–*19*). This method thus allows us to obtain recognition agents based on functional differences of the virus surface, which do not need to be known in advance. This ability is especially advantageous for the specific detection of infectious viruses, because the specific differences between infectious and noninfectious viruses, such as those rendered noninfectious through decontamination of surfaces or by the immune system in the body, are often not clearly understood, so SELEX is one of the only methods to obtain infectivity-specific recognition agents without any such foreknowledge of these differences. It has been reported that free chlorination treatment produces chemical modification on different residues of the protein on the surface of the virus while maintaining intact virus assemblies (*15*). For example, exposure of HAdV-2 to both free chlorine (*20*) and ultraviolet (UV) light (*21*) inhibited steps between attachment to the host cell and early protein RNA synthesis, most of which involving motifs of the three external capsid proteins (fiber, penton base, and hexon). Therefore, we hypothesize that, by using positive selection of aptamers that can bind infectious viruses with unmodified surface residues and counterselection to remove sequences that can bind disinfected viruses that have modified surface residues, we will be able to obtain a highly selective aptamer that can distinguish functional differences of whether the virus is infectious or not. To characterize the functional state of the virus and the concentration of HAdV that are infectious, plaque assay was used. This is the only method that can differentiate infectious from noninfectious virus, as opposed to methods based on nucleic acid detection, such as qPCR (*11*, *22*), and, thus, is the assay that is used in this work to benchmark our results.

To monitor the selection progress, we used the qPCR technique to measure both the elution yield, defined as the amount of single-stranded DNA (ssDNA) bound to infectious HAdV divided by the total amount of added ssDNA (fig. S1A), and the shift in melting curves after qPCR to assess sequence diversity of the DNA pools (fig. S1B) (*23*). We then used high-throughput sequencing (HTS) to analyze the sequences from several selection rounds, allowing us to track the evolution of individual sequences over multiple selections rounds, and to identify "winner" aptamer sequences that are enriched with subsequent rounds, using the FASTAptamer analysis toolkit (*24*, *25*). From this analysis, we identified a sequence, named HAdV-Seq4, that has been enriched over consecutive selection rounds (fig. S1C) and predicted its secondary structure using UNAFold (fig. S1D).

To characterize the binding affinity of HAdV-Seq4 to the virus target, we used both enzyme-linked oligonucleotide assay (ELONA) to obtain a dissociation constant (K_d) of (0.9 ± 0.1) nM (Fig. 1B), which is at least one order of magnitude stronger than K_d's of previously reported aptamers for other viral particles (*26*–*28*), and thermofluorimetric analysis (TFA) (*29*, *30*) to obtain a K_d of (3.6 ± 0.6) × 10^4 plaque-forming units (pfu)/ml (fig. S2A, purple). For both assays, noninfectious HAdV gave a much lower signal (Fig. 1B and fig. S2B). The above results strongly suggest that the HAdV-Seq4 aptamer has a remarkably high affinity and selectivity for infectious HAdV over noninfectious HAdV.

To meet the ultrahigh sensitivity required for virus detection, we integrated the aptamers into solid-state nanopores (*31*, *32*). Recognition elements, such as synthetic peptides, have previously been incorporated into nanopores to gain selectivity (*33*). However, with the pulsing-resistive approach used in these studies, the current signature detected still requires complex analysis to reach analyte selectivity. In contrast, single asymmetric nanochannel sensors in polymeric thick membranes can be characterized through steady-state current-voltage (*I*-*V*) measurements by sweeping the transmembrane

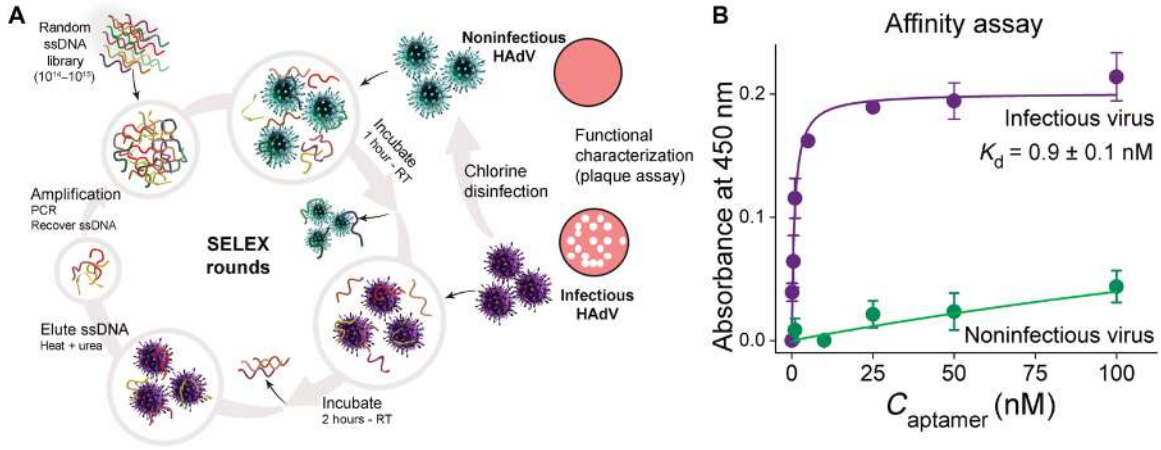

Fig. 1. In vitro selection of infectious adenovirus-specific aptamer. (**A**) Schematic representation of the in vitro selection process for HAdV. Positive and counterselection steps were added in each round to reach high specificity toward infectious virus. RT, room temperature. (**B**) Binding curves obtained from the ELONA assay. The dissociation constant (K_d) of the HAdV-Seq4 aptamer for infectious HAdV (0.9 nM) is more than 100 times higher than for noninfectious HAdV. $n = 3$ technical replicates (mean ± SD).

Table 1. DNA sequences used in this work.

Name	DNA sequence (5′ to 3′) (IDT modification in bold)
DNA library HAdV	GTCCATCGTTCGGTAGTG-**45N**-GGCTAACTGTCCACGATT
Forward primer (FwdP) HAdV	GTCCATCGTTCGGTAGTG
Reverse primer (RevP) HAdV	**/5Biosg/**AATCGTGGACAGTTAGCC
T20	TTTTTTTTTTTTTTTTTTTT
HAdV-Seq4	GGCTGCAGCTGAAGCACTGGTTTTGAGTCAAACCCAGACGATGGA
3AmMO-HAdV-Seq4	GGCTGCAGCTGAAGCACTGGTTTTGAGTCAAACCCAGACGATGGA**/3AmMO/**
NH_2-C_{12}-HAdV-Seq4	**/AmMC12/**GGCTGCAGCTGAAGCACTGGTTTTGAGTCAAACCCAGACGATGGA
DNA library SARS-CoV-2	ACCGTCAGTTACAATGCT-**45N**-GGCTGGACTATCTGTGTA
Forward primer (FwdP) SARS-CoV-2	ACCGTCAGTTACAATGCT
Reverse primer (RevP) SARS-CoV-2	**/5Biosg/**TACACAGATAGTCCAGCC
SARS2-AR10	CCCGACCAGCCACCATCAGCAACTCTTCCGCGTCCATCCCTGCTG
NH_2-C_{12}-SARS2-AR10	**/AmMC12/**CCCGACCAGCCACCATCAGCAACTCTTCCGCGTCCATCCCTGCTG

potential at low frequencies (<0.1 Hz). This method substantially simplifies the signal detection and allows direct detection of binding events that occur in sensing elements upon target recognition (*31*, *34*), resulting in remarkable signal amplification capacity, as have been demonstrated for protein, DNA (*35*, *36*), and small-molecule detection (*37*). Moreover, the steady-state *I*-*V* curves contain precise information that is essential for quantification, background subtraction, and identification of potential interfering species.

Therefore, to construct a highly sensitive sensor, we fabricated single-nanochannel membranes by irradiation of polyethylene terephthalate (PET) films with single swift heavy ions and subsequent chemical etching of the generated single-ion track. During the chemical etching process, both the shape and size of the nanopore were adjusted to obtain a single bullet-shaped nanopore with dimensions of less than 55 nm in the narrow entrance (tip) and several hundred nanometers in the opposite entrance (base) (*38*, *39*). A smaller tip size is necessary to enhance the sensitivity of the system, i.e., to enhance the variation in current signal when the virus binds to the pore. The HAdV-Seq4 aptamer was immobilized onto the inner wall of the nanopore after etching by 1-ethyl-3-(3-dimethylaminopropyl)carbodiimide/sulfo-*N*-hydroxysuccinimide (EDC/Sulfo-NHS) coupling between the carboxylate groups present on the surface of the nanopore after etching and the NH_2-modified HAdV-Seq4 aptamer (Fig. 2A and fig. S3) (*40*). To prevent the nanopore surface from interfering with the aptamer binding to its target, a spacer was added between the amine group and the aptamer (fig. S3B). The above modification procedure was verified by the *I*-*V* measurements, showing a decrease in the current after grafting the aptamer onto the nanopore (fig. S3A), due to a decrease in the effective nanochannel cross section because of the presence of the DNA.

We first determined the sensitivity of the aptamer-nanopore system for detecting HAdV by evaluating the ion transport property changes as a function of the HAdV concentrations (fig. S4). The virus samples were incorporated to the reservoir facing the base of the nanopore (900 ± 100 nm) and incubated for 30 min with the

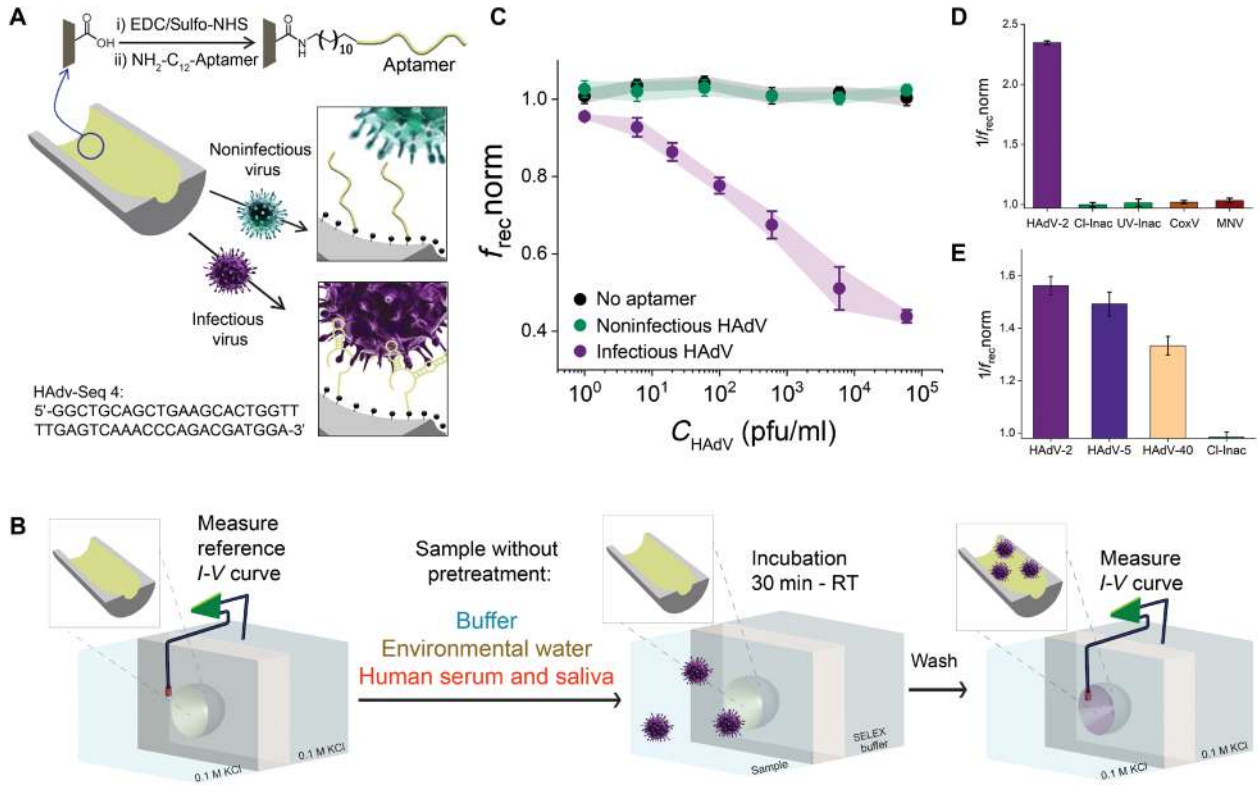

Fig. 2. Infectious HAdV detection using aptamer-functionalized nanopore sensors. (**A**) Scheme depicting the modification of the nanopore and the interaction of the aptamer with infectious HAdV samples. (**B**) Scheme of infectious HAdV detection by the aptamer-nanopore system. (**C**) Normalized rectification efficiencies (f_{rec}norm) versus virus concentration. $n = 3$ technical replicates (mean ± SD). When no aptamer was added on the nanopore (black), no change in f_{rec}norm was observed for infectious HAdV. Colors correspond to the nanopore modified with NH_2-C_{12}-Aptamer for different concentrations of noninfectious virus (green) and infectious virus (purple). (**D**) Selectivity assay. Inverse of f_{rec}norm obtained for infectious HAdV (HAdV-2), two noninfectious HAdVs using different inactivation mechanisms [free chlorine (CI-inact) and UV light (UV-inact)], and two other viruses (CoxV and MNV). The concentration of each virus is 5×10^4 pfu/ml. (**E**) Inverse of f_{rec}norm obtained for different serotypes of infectious adenovirus (HAdV-2, HAdV-5, and HAdV-40) and comparison with an inactivated HAdV sample at the same concentration (1×10^3 pfu/ml).

aptamer-nanopore system, followed by washing once with water to remove the excess of virus and then measuring the *I-V* characteristic curve in a 0.1 M KCl solution (scheme in Fig. 2B). We applied the virus samples to the reservoir facing the base of the nanopore to allow the virus to enter the nanopore and bind to the aptamer that is coated on the inside of the pore (fig. S5). The capture of the virus inside the nanopore produces a strong confinement, as the nanopore is 10 times larger than the virus, resulting in a consequent signal amplification. The rectification efficiencies (f_{rec}) were normalized by dividing each f_{rec} from the samples containing viruses by f_{rec} of the same system in the presence of just buffer ($f_{rec,0}$) to account for slight differences in the *I-V* curves characteristic for each nanopore after etching. Figure 2C shows the normalized rectification efficiency (f_{rec}norm) versus the concentration of virus. No significant change in f_{rec}norm was observed after incubation with the infectious HAdV when the nanopore was not functionalized with the aptamer (Fig. 2C, black). Once the aptamer was grafted on the inner wall of the nanopore, f_{rec}norm decreased with increasing amount of the infectious HAdV (Fig. 2C, purple), due to a change in the effective pore size with the virus incorporation and, thus, in the ion transport properties. We have quantified the infectious HAdV concentration using plaque assays and benchmarked our results with this gold standard method to quantify infectious virus, because simpler and more recently developed methods such as qPCR and immunoassays fail to determine infectivity status of the viruses (text S1) (*11*). We were able to quantify the infectious HAdV in a broad range, from 6 pfu/ml to 6×10^4 pfu/ml (fig. S6A), with the ability to detect the HAdV down to 1 pfu/ml (fig. S6B and text S2). At such a low level of detection, the diffusion of the viral particles into the nanopore can be rate limiting. To determine the contribution of mass transport on our nanopore signal experiments, magnetic stirring was incorporated during the virus incubation step (fig. S7). We found that the transport of virus to the nanopores is limiting the nanopore signal only for concentrations lower than 20 pfu/ml. However, incubation for 30 min was sufficient to obtain enough signal for detection due to the high sensitivity of the nanopore.

To demonstrate the selectivity of our aptamer-nanopore sensor, we measured the rectification current in the presence of only noninfectious HAdV and other viruses. No significant change in f_{rec}norm was observed in the presence of a wide range of concentrations of noninfectious HAdV (Fig. 2D) after incubating them for 30 min, indicating high selectivity against noninfectious HAdV. Moreover, the sensor also shows remarkable selectivity against UV light–inactivated HAdV-2 (UV-inact), as well as against high concentrations of other waterborne viruses: coxsackievirus B5 (CoxV) and murine norovirus (MNV) (Fig. 2D). In addition, we tested the sensor with different infectious HAdV serotypes, such as HAdV-2,

HAdV-5, and HAdV-40 (Fig. 2E). Although the HAdV-Seq4 aptamer was selected against HAdV-2, it can recognize all three different serotypes of infectious adenoviruses tested. Among the serotypes, HAdV-40 is a type of HAdV that cannot replicate well in cell culture systems and, thus, is not as readily detectable by a standard plaque assay. The fact that aptamer is able to detect other infectious HAdV serotypes supports that they may share a common structural motif that the aptamer can recognize, making it possible for our aptamer to detect many infectious HAdV serotypes, even if we select the aptamer to bind only one type. As a result, our method cannot differentiate virus subtypes in mixed samples. On the other hand, the signal obtained at the same concentration of virus is not always the same; it is particularly interesting to notice that the signal change for HAdV-2 and HAdV-5 is similar, while that for HAdV-40 is lower. This difference may correlate with slight differences in affinity as the aptamer was selected with the unique surface of HAdV-2. Overall, we successfully obtained a sensor that detect various infectious serotypes of adenoviruses, but not those that have been inactivated by disinfection methods.

Furthermore, we found that the sensor could quantify infectious HAdV in a mixture of infectious and noninfectious HAdV (fig. S8) and showed a high degree of correlation with a plaque assay as a benchmark (Fig. 3A). The ability of our sensor to quantify infectious HAdV in real environmental samples was also tested with various types of samples, including drinking water samples from tap water in Champaign (IL, USA), drinking water samples from a borehole in a secondary school in Uganda (Africa), and wastewater effluent samples (IL, USA). The three samples were measured using the sensor without any pretreatment of the water (fig. S9), and the results were compared with the plaque assay results (Fig. 3B). For both drinking water samples, the recovery yield was (102.5 ± 5.5)%, while for the wastewater effluent, the recovery yield was (95 ± 7)%, indicating that our sensor can quantify infectious HAdV in real water samples despite the presence of potential interfering background substances. Furthermore, when a 99.9% inactivated HAdV was spiked into these water samples, it was possible to quantify infectious HAdV (10 pfu/ml) in the presence of total HAdV (7×10^3 pfu/ml) in all cases (fig. S10). Overall, these results demonstrate that the performance of the aptamer-nanopore sensor is largely unaffected by the complex matrices of the real water samples.

To extend this aptamer-nanopore sensor for rapid diagnostics of infectious HAdV directly from bodily fluids, we spiked 1.5 ml of human serum and saliva with 15 μl of infectious HAdV solution of different concentrations, therefore avoiding significant dilution of the biological sample. We observed a decrease in f_{rec}norm with different concentrations of infectious HAdV (fig. S11), and their performance was similar to those measured in buffer (Fig. 3C). In our approach, the signals from interfering species in human serum and saliva samples can be removed readily by a washing step to remove those species that do not bind to the aptamer and by measuring the *I-V* curve in the sample without virus and normalizing f_{rec} to obtain the f_{rec}norm signal. These results demonstrate the advantage of obtaining the precise information contained in the *I-V* curve. This enables robust quantification, simple background subtraction, and removal of potential interferences, neither of which are possible with other nanopore methods. However, we cannot rule out the possibility of the geometry of the nanopore itself contributing as well to the results in real samples.

Because our selection method does not depend on known biomarkers to differentiate infectious and noninfectious viruses, it can be readily applied to newly emerging viruses, which have been appearing worldwide at an increasing rate, without any information about the inactivation mechanism. To demonstrate the generality of our method, we applied our sensor to detect SARS-CoV-2, the newly emerged coronavirus responsible for the COVID-19 pandemic, which has infected nearly 120 million people and resulted in more than 2.3 million deaths worldwide as of late February 2021. To retain the advantages of applying a whole-virus in vitro selection approach in applying our sensor to SARS-CoV-2, which is classified as a biosafety level 3 (BSL-3) agent, in vitro selection was performed using a pseudotyped SARS-CoV-2 virus. The pseudotyped virus is generated from a lentivirus (HIV) that displays the SARS-CoV-2 spike (S) protein within the viral envelope and thus closely mimics the surface and entry mechanism of SARS-CoV-2 but is defective in continuous viral replication (text S3) (*41*, *42*). Because our SELEX strategy to differentiate infectious from noninfectious viruses depends only on the surface of the viruses, using this pseudotyped virus allowed us to work in a BSL-2 laboratory. Because of their advantage at modeling the SARS-CoV-2 surface and entry mechanisms, requiring only a BSL-2 laboratory, pseudotyped SARS-CoV-2

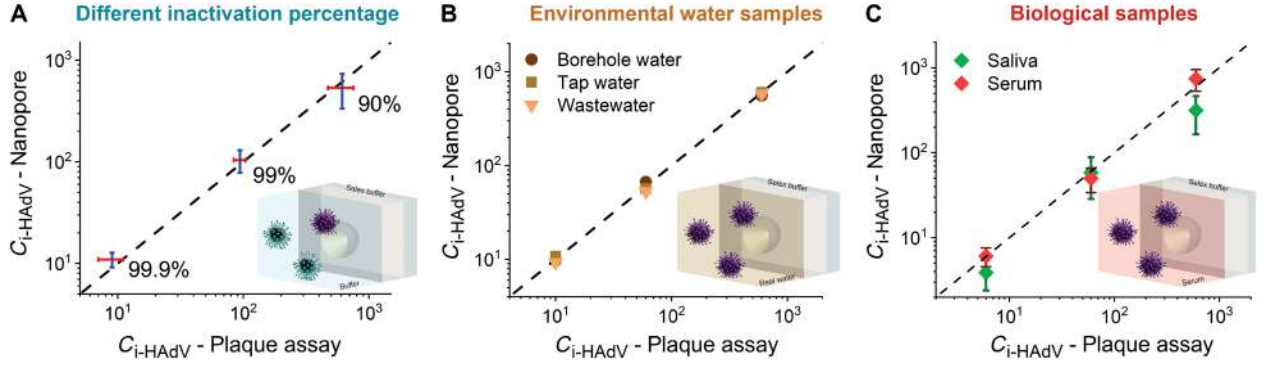

Fig. 3. Direct quantification of infectious HAdV in real samples with the aptamer-nanopore system. (**A**) Quantification of infectious HAdV in a mixture of infectious and noninfectious HAdV by comparison of aptamer-nanopore sensor (*y* axis) with plaque assay (*x* axis). (**B**) Quantification of infectious HAdV in different real water samples without any pretreatment or dilution by comparison of aptamer-nanopore sensor (*y* axis) with plaque assay (*x* axis). (**C**) Quantification of infectious HAdV in human serum and saliva without dilution of the biological sample by comparison of aptamer-nanopore sensor (*y* axis) with plaque assay (*x* axis). $n = 3$ technical replicates (mean ± SD).

has been used previously to study the cell type susceptibility, virus receptor, entry pathway, and protease priming for SARS-CoV-2 and also to identify several potential drug targets and neutralizing antibodies for SARS-CoV-2 (*43*). Thus, pseudotyped SARS-CoV-2 has been widely used as a reliable and robust model for infectivity.

To achieve high selectivity against active SARS-CoV-2 over inactive SARS-CoV-2, we performed counterselection against UV light–inactivated pseudotyped SARS-CoV-2 (fig. S12). UV inactivation produces damage in the genome and in the proteins on the surface of the virus while largely maintaining the intact virus structure. Furthermore, to obtain an aptamer with the ability to distinguish against other viruses, including very similar coronaviruses, we incorporated counterselection against a lentivirus pseudotyped with SARS-CoV-1 S protein and a lentivirus pseudotyped with influenza hemagglutinin 5 and neuraminidase 1 proteins (H5N1). Ten rounds of selection were performed (fig. S13). After sequencing different rounds with HTS, we identified a sequence, named SARS2-AR10, that showed good enrichment over subsequent selection rounds (fig. S13C). ELONA results showed a K_d of (79 ± 28) nM with high selectivity against UV-inactivated pseudotyped SARS-CoV-2 (fig. S14), and microscale thermophoresis (MST) also showed that SARS2-AR10 binds to active SARS-CoV-2 but not to UV-inactivated pseudotyped SARS-CoV-2 or other viruses such as 229E coronavirus, pseudotyped SARS-CoV-1, or pseudotyped influenza H5N1 (fig. S15), demonstrating the high selectivity of SARS2-AR10 toward active SARS-CoV-2. For COVID-19 diagnostics, it is important to differentiate between different coronaviruses; thus, strict counterselection steps were applied to tune the selectivity of the SARS2-AR10 aptamer.

To gain insights into SARS2-AR10 selectivity, we assessed the binding of our aptamer to isolated SARS-CoV-2 S1 protein in solution with and without UV treatment using ELONA assay to measure the binding curve. Figure S16 shows that SARS2-AR10 binds to the active S1 domain with a lower affinity than toward pseudotyped SARS-CoV-2. This is an expected result because the aptamer was selected using the pseudovirus, which mimics SARS-CoV-2 spike protein in its native conformation, and thus, it likely binds better to the accessible surface residues of the spike protein of SARS-CoV-2, but not those embedded within the envelope of the pseudovirus. In addition, because the trimeric spike protein assembles on the surface of the virus in trimers, our aptamers likely bind these spike proteins, but not necessarily individual spike protein. Furthermore, the affinity of the aptamer toward the UV-inactivated S1 protein is lower. These results suggest that the specificity is mainly achieved through protein recognition and inactivating modifications.

We then determined the ability of the SARS2-AR10–nanopore system to detect and quantify SARS-CoV-2 with different concentrations of active pseudotyped SARS-CoV-2 after 30 min and 2 hours of virus incubation (fig. S17). An increase in the virus incubation time resulted in a higher sensitivity and lower detection limit. With 2 hours of incubation, the sensor detected as low as 1×10^4 copies/ml and quantified a broad range of virus concentrations, from 1×10^4 to 1×10^8 copies/ml (Fig. 4A). Thus, our method can reach the lowest detectable concentrations in individuals that have tested positive for SARS-CoV-2 in saliva and nasal swabs (*1*). Furthermore, the lowest detectable concentration of our method (1×10^4 copies/ml) is similar to the detection limit reached by reverse transcription PCR (3×10^3 copies/ml) (*44*) and other nucleic acid detection methods, for instance, those based on LAMP (loop-mediated isothermal amplification) reaction (5×10^4 copies/ml) (*2*, *45*). We further tested the selectivity of our aptamer-nanopore sensor against inactive SARS-CoV-2 (Fig. 4A) and against an endemic coronavirus that produces the common cold, 229E coronavirus, as well as pseudotyped SARS-CoV-1 and H5N1 influenza virus (Fig. 4B) and found no substantial change, supporting the high selectivity of our sensor for active SARS-CoV-2 against inactive SARS-CoV-2, other coronaviruses, and influenza virus.

Last, we spiked 12 human saliva samples with different concentrations of active pseudotyped SARS-CoV-2 and observed a decrease in f_{rec}norm with different concentrations of active SARS-CoV-2 (fig. S18). The results show a good correlation between the concentration calculated using the obtained f_{rec}norm in saliva compared with the concentration measured with luciferase assay (Fig. 4C), indicating that our aptamer-nanopore system can quantify pseudotyped SARS-CoV-2 in saliva without any pretreatment of the biological sample. When we immobilized a control sequence in the nanopore and repeated the experiment under the same conditions with a high concentration (1×10^7 copies/ml) of spiked pseudotyped

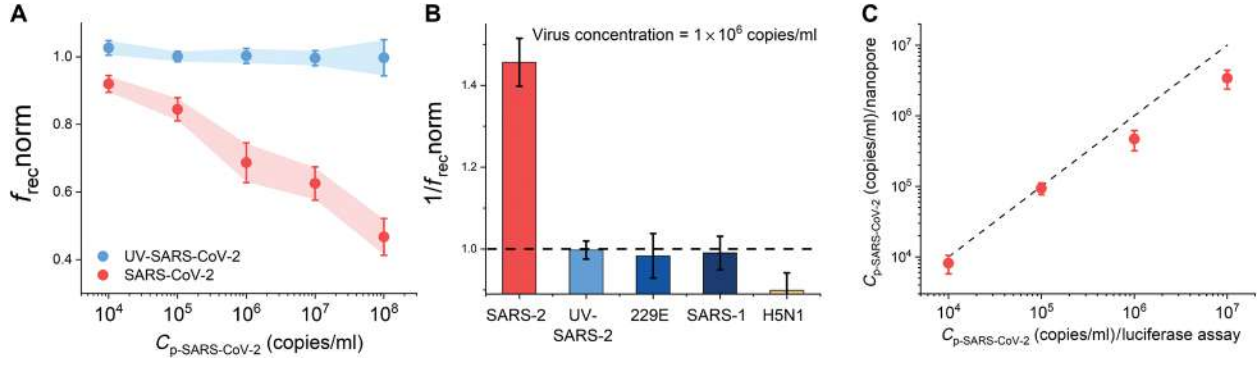

Fig. 4. Quantification of active pseudotyped SARS-CoV-2 with the aptamer-nanopore system. (**A**) Normalized rectification efficiencies versus virus concentration. $n = 3$ technical replicates. Colors correspond to the nanopore modified with different concentrations of UV-inactivated pseudotyped SARS-CoV-2 (blue) and active pseudotyped SARS-CoV-2 (red). (**B**) Selectivity assay. Inverse of f_{rec}norm obtained for active pseudotyped SARS-CoV-2 (SARS-2), UV-inactivated pseudotyped SARS-CoV-2 samples (UV-SARS-2), another coronavirus (229E), and two other pseudoviruses [SARS-CoV-1 (SARS-1) and influenza virus (H5N1)]. The concentration of each virus is 1×10^6 copies/ml. (**C**) Comparison of aptamer-nanopore sensor (*y* axis) with luciferase assay (*x* axis) to quantify active pseudotyped SARS-CoV-2 in human saliva without dilution of the biological sample. $n = 3$ technical replicates (mean ± SD). Each of these measurements was performed with a new membrane.

SARS-CoV-2 in saliva, we observed no substantial change in the nanopore signal (fig. S19). Therefore, the changes in f_{rec}norm are related to the specific binding of SARS-CoV-2 to the aptamer.

DISCUSSION

The sensitivity of our method rivals those for standard viral assay methods such as the plaque assay and qPCR, with the major advantage being that it is much faster (30 min to 2 hours), as we do not need to wait for plaques to fully develop (e.g., 10 days for HAdV) or the genome to be extracted and replicate (e.g., 24 hours for HAdV). In addition, our method can detect infectious viruses that cannot replicate well in cell culture systems, such as HAdV-40, and thus are not readily detectable by the standard plaque assay. The sensitivity enhancement and low limit of detection (LOD) obtained with the aptamer-nanopore may be related to two main factors. First, viruses are known to present multiple antigens (e.g., S protein for SARS-CoV-2) on the surface and thus multiple identical binding sites for the aptamers. Thus, this multivalent binding avidity can increase the sensitivity, as reported previously (*46*). In addition, it has been demonstrated that the presence of charged groups on the nanopore walls, such as DNA aptamers, can lead to strong ionic preconcentration effects inside the nanopore. Such a nanoconfinement effect is also known to increase the sensitivity (*47*, *48*).

In comparison to qPCR or other nucleic acid detection–based tests, our system can detect intact viruses directly in real samples, without the need to collect and disrupt the viruses for nucleic acid extraction, thereby resulting in high selectivity against noninfectious virus. In addition, these simpler and more recently developed methods based on nucleic acid detection cannot inform virus infectivity, and thus, in this work, the only gold standard method available to benchmark our aptamer-nanopore sensor was the plaque assay.

We choose free chlorine as the disinfection method for HAdV-2 in water, because it is the most common disinfection method for treatment of water samples. To demonstrate that the same method of SELEX can be applied to other disinfection methods, we further showed that our method could also distinguish active from UV-inactivated SARS-CoV-2 pseudovirus, suggesting that we can achieve selectivity regardless of which of these two procedures are used for inactivation. Furthermore, because our aptamer can differentiate infectious from noninfectious viruses, a detailed characterization of the binding targets of our aptamers can also be applied to reveal surface changes responsible for the loss of infectivity for each of the inactivation treatment.

We were able to successfully apply the aptamer-nanopore system to two different types of viruses, showing the broad application range of our approach. On the one hand, the HAdV is a nonenveloped virus, with a protein capsid as the surface, which makes it more rigid and probably with a compact surface charge, while SARS-CoV-2 is an enveloped virus, where the surface consists of a more flexible lipid bilayer in which surface proteins are embedded. These surface differences can affect the nanopore response, which is highly dependent on the charge and size of the target. These viruses' differences as well as differences in the binding affinities of the aptamers, where HAdV-Seq4 has 80 times stronger affinity than SARS2-AR10, can explain the different responses in terms of virus incubation time and analytical performance. Thus, further optimization of the aptamer sequence could help to decrease the incubation time needed to reach the same sensitivity and detection limit for SARS2-AR10 as for HAdV-Seq4. In addition, because several aptamers for the spike protein, S1 domain, or RBD (receptor binding domain) of the spike protein of SARS-CoV-2 have been reported (*49*–*51*) since our work has begun, immobilizing these aptamers into the nanopore could further enhance LOD and sensitivity.

Furthermore, our SELEX strategy to differentiate infectious from noninfectious viruses depends only on the surface of the viruses; thus, aptamer selection can proceed on pseudotyped viruses, lessening the need of working with new emerging pathogens that are classified as BSL-3 with very restricted worldwide availability for whole virus experiments. We propose that our workflow for aptamer selection against SARS-CoV-2 using a pseudotyped virus that can mimic the native state of the surface proteins may well be applicable as a whole virus selection strategy for other emerging pathogens.

These results demonstrate the enormous design flexibility offered by our aptamer-nanopore sensors. The implementation of SELEX to obtain specific aptamers for infectious viruses and their subsequent assembly into the corresponding aptamer-nanopore systems, where the steady-state *I-V* curves contain precise information that allows quantification and background subtraction, make it possible to quantify viruses in samples ranging from complex environmental samples to untreated biological fluids, which will allow a wide range of applications for rapid and selective detection of both current and emerging viral pathogens around the world.

MATERIALS AND METHODS

DNA library

All the DNA sequences were purchased as synthetic oligonucleotides from Integrated DNA Technologies (IDT). A random ssDNA library (1 nmol) and reverse and forward primers were purified by polyacrylamide gel electrophoresis.

The ssDNA pool consisted of a central random region of 45 nucleotides flanked by two constant sequences at the 3′ and 5′ ends that act as primer regions for amplification (see Table 1). The reverse primer was modified with biotin to separate ssDNA from amplified double-stranded PCR products using streptavidin-coated beads during the in vitro selection process. Unmodified FwdP and RevP were used for PCR amplification after the final round of the in vitro selection, for HTS library preparation, and for qPCR quantification. Proper folding of ssDNA library and pools was attained by denaturing at 95°C for 10 min, followed by cooling on ice for 10 min before use in each round.

HAdV propagation and viability assessment

HAdV-2 (VR-846) was propagated with A549 cells (CCL-185), both obtained from the American Type Culture Collection (ATCC; Manassas, VA). Cell incubation, viral propagation, and viral infectivity assessment methods were similar to previously reported protocols (*20*). Briefly, A549 cell monolayers were maintained in flasks at 37°C with 5% CO_2 with modified Ham's F12K media + 10% fetal bovine serum + amphotericin B (0.25 μg/ml) + penicillin (100 U/ml) + streptomycin (10 μg/ml) (Sigma-Aldrich, St. Louis, MO). To propagate the viruses, HAdV-2 liquid stock was inoculated onto A549 cell monolayers and incubated at 37°C with 5% CO_2 until cytopathic effects showed up. Viruses were released from the cells by freeze-thaw cycles. The lysates were centrifuged, and the

supernatants were passed through 0.45- or 0.22-μm vacuum filters to remove large debris (Millipore, Billerica, MA). The filtrate was purified and concentrated using a 300-kDa ultrafiltration membrane (Millipore) in Amicon stirred cells. For some later batches of propagation, the filtrate was purified and concentrated using sucrose cushion ultracentrifugation. The concentrated virus stocks were in 1 mM carbonate buffer solution (CBS; Thermo Fisher Scientific) stored at −80°C. The virus infectivity was assessed with soft agar overlay plaque assay, and plaque counting at 9 or 10 days after infection was used to determine virus titers.

Inactivation of HAdV—Chlorine treatment

The inactivation of HAdV-2 by free chlorine was previously described (*15*, *20*). Briefly, a batch reactor with 1 mM CBS under continuous magnetic stirring was spiked with HAdV-2. The temperature was maintained constant with a water bath, and pH was adjusted with hydraulic acid or sodium hydroxide solution. An initial sample was taken to measure initial viral concentration with the plaque assay method and then sodium hypochlorite solution was added into the reactor while a timer was started at the same time. Samples were taken along with time and immediately mixed with 0.1% sodium thiosulfate to quench the chlorine and stop the inactivation process. The time points at which samples were added into sodium thiosulfate were recorded. Although the initial sample had no chlorine, it was also mixed with 0.1% sodium thiosulfate so that all the samples are comparable. The chlorine concentration was monitored with the *N*,*N*-diethyl-*p*-phenylene diamine method (*52*), and the sampling times and chlorine concentrations were both recorded. Chlorine reacts extremely fast with viruses, leaving no time to measure the initial chlorine concentration in this reactor, so a second reactor controlling for the addition of virus stock was prepared to make the measurement of initial chlorine concentration possible.

The inactivated HAdV was dialyzed with 1 mM CBS buffer to remove the excess of sodium hypochlorite and sodium thiosulfate. In this way, the infectious and noninfectious HAdV are in the same buffer for the in vitro selection process.

Inactivation of HAdV-2 by low-pressure UV light

The UV light inactivation experiments followed previously published methods except that a low-pressure UV lamp (GSL233T5L/SL, Atlantic Ultraviolet Corporation, Hauppauge, NY) was operated at 10 W and no band-pass filters were installed. A recirculating water-jacketed reactor (20°C) containing 1 mM CBS was spiked with HAdV-2 under continuous magnetic stirring. The fluence was calculated as the product of the average irradiance and exposure time, and four factors were measured for necessary corrections based on the literature (*53*). The irradiance distribution across the irradiated water surface was measured with a 1400A radiometer and a SEL240 detector (International Light Technologies, Peabody, MA) to correct for the nonuniformity of the light distribution (petri factor). The UV absorbance at 254 nm of the water sample to be treated by UV was measured with a UV-2700 Shimadzu spectrophotometer to adjust for water depth because UV can be absorbed by water (water factor). Distance of suspension from the UV lamp (divergence factor) and water surface reflection (reflection factor) were also considered into the calculation. With the average irradiance obtained and the desired fluence, the required exposure time was obtained.

Other waterborne viruses

Other viruses tested in this study include HAdV-5, HAdV-40, CoxV, and MNV. HAdV-5 (VR-5) was obtained from ATCC, and its propagation method and viral infectivity assessment are the same as those described for HAdV-2. HAdV-40 (Ad40, Dugan strain, p.3, clone 6A) was obtained from T. Cromeans (Centers for Disease Control and Prevention) (*54*). Coxsackievirus B5 Faulkner (VR-185) was obtained from ATCC and passaged in buffalo green monkey kidney cell (Quidel, San Diego, CA) monolayers three times and then purified and concentrated following the protocol of HAdV-2. Murine norovirus was originally provided by H. Virgin (formerly at Washington University School of Medicine, St. Louis, MO) and propagated using RAW 264.7 cells (TIB-71) obtained from ATCC. The virus purification and concentration protocol were similar to those of HAdV-2.

Cell culture for pseudovirus production

293T embryonic kidney cells (ATCC, no. CRL-1573) and human hepatoma cell line Huh-7 (obtained from T. Gallagher at Loyola University) were cultured in Dulbecco's modified Eagle's medium (DMEM) supplemented with 10% fetal bovine serum (Gibco), 100 U of penicillin, and streptomycin (100 μg/ml) (Invitrogen).

Production and quantification of pseudotyped viruses

Pseudoviruses were created using the following plasmids: SARS-CoV-1 spike protein, SARS-CoV-2 spike protein, hemagglutinin, and neuraminidase isolated from the highly pathogenic avian influenza virus A/Goose/Qinghai/59/05 (H5N1) strain and the HIV-1 proviral vector pNL4-3.Luc.R-E- (obtained through the National Institutes of Health AIDS Research and Reference Reagent Program). All pseudovirions were produced by transient cotransfection of 293T cells using a polyethyleneimine-based transfection protocol. Five hours after transfection, cells were washed with phosphate-buffered saline (PBS), and 20 ml of fresh medium was added to each 150-mm plate. Twenty-four hours after transfection, the supernatant was collected and filtered through a 0.45-μm pore size filter. Pseudotyped virus was concentrated by ultracentrifugation. The pseudovirus was layered onto a 30% (w/v) sucrose cushion and centrifuged at 26,000 rpm for 2 hours in a Thermo Fisher Scientific AH-629 rotor. The pelleted pseudovirus was resuspended in sterile PBS, aliquoted, and frozen for future use. The pseudovirus titer was determined using a quantitative p24 lentivirus ELISA kit (Takara Lenti-X p24 Rapid Titer Kit, catalog no. 632200).

UV inactivation of pseudotyped SARS-CoV-2

We targeted 293T cells that were transfected with pcDNA3.1(+)-ACE2 and pCSDest-TMPRSS2 for 6 hours. The cells were then trypsinized and seeded at 1×10^5 cells per well in DMEM complete into white-bottom 96-well plates (100 μl per well) and then incubated for 16 hours at 37°C and 5% CO_2. To evaluate the efficacy of UV irradiation of the SARS-CoV-2 pseudotyped virus, the pseudovirus was placed in an open plastic petri dish and positioned under the UV light source in a biosafety cabinet and irradiated at differing time points with 134 μW/cm^2. The UV-treated pseudovirus containing a luciferase reporter gene was added to the 96-well plates along with non–UV-treated pseudovirus as a control. Plates were incubated at 37°C and 5% CO_2 for 48 hours, and viral infection was determined by luminescence using the neolite reporter gene system (PerkinElmer). Data were normalized to non–UV-treated pseudovirus (100% infectivity).

Production and quantification of infectious 229E coronavirus

229E coronavirus was obtained as a gift from T. Gallagher (Loyola University). The virus was propagated in Huh-7 cells, and stocks were frozen at −80°C. For quantification, approximately 1×10^6 Huh-7 cells per well were seeded in six-well tissue culture plates (Corning) and allowed to grow to 90% confluence for 24 hours. Viral stocks were serially diluted 10-fold (10^{-2} to 10^{-8}); culture medium was removed and replaced with 400 μl of each viral stock dilution in triplicate. Plates were incubated at 33°C, 5% CO_2 for 2 hours, rocking gently every 20 min. After 2 hours, the virus was removed and replaced with 2 ml of a 1:1 mixture of 2× MEM and 2.4% Avicel-591. Plates were incubated at 33°C, 5% CO_2 for 96 hours. Plates were fixed with 10% formalin and stained with 1% crystal violet to visualize plaques.

Water samples and biological samples

Tap water was obtained from the tap at the University of Illinois at Urbana-Champaign (UIUC), in Illinois, USA. A more complex drinking water sample was obtained from a borehole at Panyodoli Secondary School in Kiryandongo District, Uganda. Wastewater secondary effluent was obtained from Urbana and Champaign Sanitary District in Illinois, USA.

Human serum from human male AB plasma (USA origin, sterile-filtered) was purchased from Sigma-Aldrich. Pooled human saliva samples were purchase from BioIVT.

In vitro selection of the virus-specific aptamers

A schematic diagram of the in vitro selection process is shown in Fig. 1A.

First round of in vitro selection

The heat-denatured ssDNA library (1 nmol) was mixed with 50 μl of infectious virus (6×10^5 pfu/ml) in a total volume of 350 μl of SELEX buffer [20 mM tris, 100 mM NaCl, and 2.5 mM $MgCl_2$ (pH 7.2)] and incubated for 2 hours at room temperature. Then, the unbound sequences were removed using an Amicon Ultra-0.5 100-kDa filter, followed by washing four times with 400 μl of SELEX buffer to ensure removal of all unbound sequences. To elute the bound sequences, we heated the filter containing the virus and bound sequences for 15 min at 95°C in the presence of 8 M urea and then centrifuged, collecting the fraction that flowed through the filter in a new tube. Then, to concentrate and desalt the DNA, we used an Amicon Ultra-0.5 10-kDa filter and washed two times with SELEX buffer (300 μl each time). We took 1 μl of the eluted ssDNA to quantify the amount of DNA by qPCR, and the remaining pool was used as a template for amplification of bound sequences by PCR (30 cycles of 1 min at 95°C, 30 s at 52°C, 1 min at 72°C, followed by 10 min at 72°C) to obtain the dsDNA pool. The PCR was carried out in a total volume of 50 μl with the reverse primer labeled with a biotin, using a GoTaq Flexi DNA polymerase (Promega). Last, ssDNA was recovered by streptavidin-coated magnetic beads. We took 1 μl of the recovered ssDNA to quantify the amount of DNA by qPCR, and the remaining DNA was used for the following round.

Second to 11th round of in vitro selection

Enriched pools (200 pmol) were heat-denatured as described before and mixed with 25 μl of noninfectious virus (1×10^5 pfu/ml) in a total volume of 100 μl of SELEX buffer as the counterselection step. After incubation for 1 hour at room temperature, the unbound sequences were recovered using an Amicon Ultra-0.5 100-kDa cutoff and washed two times with 100 μl of SELEX buffer. We collected the unbound sequences that flowed through the filter and incubated them with 50 μl of infectious virus (6×10^5 pfu/ml) in a total volume of 350 μl as the positive selection step. From here, the protocol is the same as for round 1 for sequence elution, desalting, and PCR amplification.

All Amicon Ultra-0.5 filters were treated with 1 mM T20 for 30 min to avoid nonspecific adsorption of the library and pool sequences on the filter, followed by washing for three times with SELEX buffer. A new PCR using unlabeled primers was performed to prepare the pools for HTS.

The in vitro selection process to obtain an aptamer specific for infectious SARS-CoV-2 was performed using the same procedure as for HAdV, with the following changes. In this case, pseudotyped SARS-CoV-2 (1×10^8 copies/ml) was used in the positive selection rounds, while UV-inactivated pseudotyped SARS-CoV-2, pseudotyped SARS-CoV-1, and pseudotyped H5N1 were used for counterselection steps (5×10^9 copies/ml of each). The SELEX buffer was 1× PBS, with 2.5 mM $MgCl_2$ and 0.5 mM $CaCl_2$ (pH 7.4). To increase the yield from the pool elution step from the 100-kDa filter, instead of eluting in 8 M urea, elution was performed in the SELEX buffer, at 95°C for 10 min. This allowed us to directly use this eluted sample without concentration/desalting with the 10-kDa filter.

In vitro selection monitoring

qPCR was used to monitor the SELEX process in two ways: (i) testing the enrichment of the pools (elution yield) using an absolute quantification and (ii) assessing sequence diversity of the pools (convergence of the aptamer species) by monitoring the melting curve (*23*). Real-time PCR experiments were conducted with the CFX96 Real-Time PCR System (Bio-Rad) according to the manufacturer's instructions. All reactions were performed in 10 μl of reaction volumes in 96-well plates for PCR. A standard qPCR mixture contained 5 μl of SsoFast EvaGreen Supermix (Bio-Rad), 0.3 μl of 500 nM of each unlabeled primer, 3.4 μl of H_2O, and 1 μl of DNA template. Thermal cycling consisted of an initial denaturation at 98°C for 2 min followed by 40 cycles of denaturation at 98°C for 5 s and annealing and extension at 52°C for 10 s. After these amplification cycles, the melting curve analysis was performed from 65° to 95°C. Threshold cycle (C_t) values were determined by automated threshold analysis.

HTS of selection rounds

Selected selection cycles (rounds 4, 6, 7, 8, 9, 10, and 11 for HAdV selection and rounds 3, 5, 7, 8, and 9 for SARS-CoV-2 selection) were prepared for HTS analysis on an Illumina HiSeq 4000 platform (performed by the DNA Services Lab of the Roy J. Carver Biotechnology Center at UIUC), using the Celero DNA-Seq Kit (Nugen/Tecan) for library preparation. Briefly, library preparation involved first performing end repair of fragmented DNA, followed by adaptor ligation, and PCR amplification to produce the final libraries. This kit incorporated different unique dual indexes that allowed the sample analysis of all rounds on one lane. After purification of the PCR product with Agencourt AMPure XP Beads (Beckman Coulter), quantification of the DNA was carried out using a fluorescence method (Qubit kit dsDNA Broad Range), and approximately equal amounts of each library containing specific indexes were mixed. After a quality control (qPCR quantification and fragment analyzer of the DNA, performed by the DNA Services Lab), 100–base pair single-end sequencing was carried out.

After demultiplexing, HTS data were analyzed using the FASTAptamer software (*24*). FASTAptamer-Count allows us to count the number of times each sequence is sampled from a population and then rank and sort the sequences by abundance, while FASTAptamer-Enrich was used to calculate fold enrichment for each sequence present in more than one round of the selection by comparing the RPM (reads per millions) of the sequence from one population by the RPM in another.

Binding affinity tests

Enzyme-linked oligonucleotide assay

ELONA was used to determine the binding affinity of the HAdV-Seq4 aptamer toward HAdV and the SARS2-AR10 aptamer to pseudotyped SARS-CoV-2. Infectious HAdV (6×10^5 pfu/ml) or active pseudotyped SARS-CoV-2 (5×10^8 copies/ml) was coated on a microplate at room temperature for 2 hours. After blocking with 100 µl of 5% bovine serum albumin in PBS for 1 hour at room temperature, the biotin-labeled aptamer was added to the individual wells at various concentrations (0.1 to 1000 nM) in the SELEX binding buffer and incubated for 1 hour at room temperature. Horseradish peroxidase–conjugated streptavidin (1:500) was added and incubated for 45 min. Color development was achieved by adding tetramethylbenzidine chromogen substrate. After adding 2 M H_2SO_4 as stop solution, the optical density at 450 nm was determined using a microplate reader. The same procedure was done for the free chlorine–inactivated HAdV and UV-inactivated pseudotyped SARS-CoV-2. For ELONA assay using the S1 protein, the same procedure was repeated, but the microplate was coated with SARS-CoV-2 spike protein S1 (Invitrogen, aa11-682).

Thermofluorimetric analysis

TFA measures the fluorescence of a mixture of DNA and intercalating dye as a function of temperature (*29*, *30*). Intercalating dyes are only highly fluorescent when bound to dsDNA. At high temperatures, double-stranded regions of the DNA dehybridize and the fluorescence decreases. TFA monitors aptamer melting, leveraging the changes in thermodynamic stability afforded by target binding.

TFA was used to test the binding of HAdV-Seq4 aptamer to HAdV. A solution containing 20 nM of aptamer was annealed at 95°C and cooled down slowly at room temperature. Then, a mixture of 2 µl of the aptamer solution, 2 µl of SYBR Gold (1:100 dilution), and 15 µl of HAdV solution at different concentrations was added to individual wells. All sets of samples were placed in the qPCR instrument, and melting curve data were acquired in triplicate, between 20° and 95°C, at 0.5°C per minute with data collection at 30-s intervals. Figure S2 shows the melting curves at different conditions.

A control experiment was carried out in the same conditions but without the HAdV-Seq4 aptamer to determine the background signal contribution from just HAdV virus. In addition, a negative control was performed by replacing the HAdV-Seq4 aptamer with a nonspecific DNA, containing the same length but a random sequence, to confirm that the detected changes corresponded to the specific interaction between HAdV-Seq4 aptamer and the infectious HAdV. Last, a selectivity test was performed by repeating the assay with the HAdV-Seq4 aptamer using a different virus commonly present in water samples, coxsackievirus.

Microscale thermophoresis measurements

MST was used to test the binding of SARS2-AR10 aptamer with pseudotyped SARS-CoV-2 and other related viruses. A 1:2 serial dilution of 16 samples of the virus with SELEX buffer was prepared, covering the concentration range of 3.9×10^8 to 4.8×10^4 copies/ml. To 10 µl of each of the serial dilutions, 10 µl of 500 nM stock solution of fluorescein-functionalized SARS2-AR10 was added and allowed to incubate for 10 min at room temperature. Subsequently, each sample was loaded onto a NanoTemper (Munich, Germany) KM-022 capillary tube and mounted on a NanoTemper Monolith Nt.115 (provided by the UIUC Microbiology Department) capillary tray. Each measurement was tested at a light-emitting diode power of 20% at the "Blue" excitation wavelength setting, with a cold region of 5 s, followed by a hot region of 30 s, until the new hot equilibrium state was observed, followed by five more seconds of cold region to observe the regeneration of the fluorescence signal. For each MST measurement, each capillary was subjected to an infrared laser power at 40% of its power to record the resulting thermophoretic curves. Each of these measurements included three repeat experiments. To test the selectivity of the aptamer, the same experiment was performed with UV-inactivated pseudotyped SARS-CoV-2, pseudotyped SARS-CoV-1, pseudotyped H5N1, and 229E coronavirus.

Nanopore fabrication

PET foils (12 µm) are irradiated at the UNILAC (Universal Linear Accelerator) heavy ion accelerator of the GSI Helmholtz Centre for Heavy Ion Research with single GeV Au ion. Each highly energetic ion creates a highly localized damage trail, known as ion track, along its trajectory through the polymer foil. The ion track has a diameter of a few nanometers and can be selectively removed by chemical etching. Chemical etching is performed in a custom, in-house-built electrochemical cell such that the irradiated foil is inserted between two separate compartments. The compartments are filled with 6 M NaOH and 6 M NaOH + 0.05% (in volume) DOWFAX 2a1, respectively. Etching is performed for 6 min at 60°C to fabricate bullet-like shaped nanochannels, i.e., a combination of longer cylindrical and shorter parabolic segments. Single nanochannels with bullet-like shape exhibit nonlinear *I-V* characteristics because of the asymmetric shape of the reduced size tip and the negative charges stemming from the carboxylate groups generated on the polymer surface during the etching. Average dimensions of the as-obtained bullet-like shaped nanochannels are (i) tip ≤ 55 nm and (ii) base of 900 ± 100 nm, as described previously (*39*).

Modification of nanopore and immobilization of the aptamer

After etching, the single nanochannel membranes were modified with the HAdV aptamer by EDC/Sulfo-NHS coupling between the carboxylate groups in the nanopore and an amino-modified HAdV-Seq4 aptamer. We chose to incorporate the amino modification at the 5′ end with the longest linker available from IDT (12 CH_2-groups) to minimize the potential for the nanopore surface to interfere with aptamer binding to its target (NH_2-C_{12}-HAdV-Seq4; see Table 1). For HAdV-Seq4 aptamer, we also incorporated the amine modification at the 3′ end to compare the effect of the different orientation of the HAdV aptamer on the surface (fig. S3). In this case, only a shorter linker (6 CH_2-groups) was available from IDT (3AmMO-HAdV-Seq4; see Table 1).

The PET single-nanochannel membrane was incubated first with 20 mM EDC and 30 mM Sulfo-NHS in reaction buffer [100 mM MES (pH 5.5)] for 45 min at room temperature to form the Sulfo-NHS esters. In the second step, after washing with the same buffer, the membrane is incubated overnight (≥6 hours) with a solution of 2 µM amino-DNA in reaction buffer at room temperature. NH_2-C_{12}-SARS2-AR10 aptamer was incorporated in the nanopore following the same procedure as for HAdV-Seq4.

I-V measurements

I-V curves were recorded using a potentiostat (CHI620, CH Instruments) in a four-electrode setup (working, working sense, reference, and counter electrode). In this way, we can monitor conductance variations arising from changes in the nanochannel and separate them from other processes in solution or on electrode surfaces. Both the working and counter electrode were platinum wires, while the reference and working sense were commercial silver/silver chloride (Ag/AgCl/3 M KCl) electrodes. In all experiments, working and counter electrodes were placed at the tip and base of the channels, respectively. A 0.1 M KCl solution was used as the electrolyte.

Measurement of the virus samples

The sample (1.5 ml) containing the virus was incorporated in the compartment facing the base of the aptamer-modified nanochannel, while a SELEX buffer was filled in the compartment facing the nanopore tip. The solutions were incorporated by pipetting into the chambers using a plastic pipette. After incubation for the given time (30 min or 2 hours), the solutions were removed, and the compartments were rinsed with Milli-Q water. Then, the 0.1 M KCl electrolyte was inserted in both compartments to record the *I-V* characteristics between +1 and −1 V at 100 mV/s (three cycles).

In the case of the environmental water and human serum and saliva samples, 15 µl of different dilutions of infectious virus (HAdV or pseudotyped SARS-CoV-2) was spiked in 1.5 ml of these samples to obtain the final concentration of spiked viruses. The dilutions of the infectious virus were prepared using SELEX buffer to dilute the HAdV stock solution (6×10^5 pfu/ml) (in CBS buffer) or pseudotyped SARS-CoV-2 stock solution (1×10^{11} copies/ml) (in PBS buffer). For the environmental water samples, the final viral titers tested were 10, 60, and 600 pfu/ml of HAdV, while for human serum and saliva, 6, 60, and 600 pfu/ml of HAdV were tested. In the case of SARS-CoV-2, the final viral titers tested were 1×10^4, 1×10^5, 1×10^6, and 1×10^7 copies/ml. For each concentration of virus, three replicates are measured using single-use aptamer-nanopore system and independently prepared virus solutions from a virus stock. From these replicates, two of them were done with the pooled saliva samples we have purchased, and the third replicate was done with individual fresh saliva samples. No signal differences were observed between these two types of saliva samples.

Rectification efficiency

In all experiments, the definition for f_{rec} is given by

$$f_{rec} = \pm\left|\frac{I(1V \text{ or } -1V)}{I(-1V \text{ or } 1V)}\right|$$

where the current I in the numerator corresponds to the largest current value in the high conductance state, and the current in the denominator is the lowest current value corresponding to the low conductance state. In addition, if the higher current corresponds to a negative voltage, the rectification factor is multiplied by −1. This definition simplifies the notation. To compare results stemming from different nanopores, f_{rec}norm is defined by dividing each f_{rec} from a specific nanochannel by the f_{rec} value in the presence of 0.1 M KCl after incubation with just buffer ($f_{rec,0}$)

$$f_{rec}\,\text{norm} = \frac{f_{rec}}{f_{rec,0}}$$

In the case of human serum and saliva samples, f_{rec}norm is calculated by dividing each f_{rec} from a specific nanochannel by the f_{rec} value of that nanochannel in the presence of 0.1 M KCl after incubation with human serum or saliva ($f_{rec,0}$). Thus, the steady-state *I-V* curves and the rectification factor obtained based on this curve contain precise information that is essential for quantification and background subtraction to remove potential interference from other species in the sample, which is not possible with other nanopore methods.

SUPPLEMENTARY MATERIALS

Supplementary material for this article is available at https://science.org/doi/10.1126/sciadv.abh2848

View/request a protocol for this paper from *Bio-protocol*.

REFERENCES AND NOTES

1. D. Jacot, G. Greub, K. Jaton, O. Opota, Viral load of SARS-CoV-2 across patients and compared to other respiratory viruses. *Microbes Infect.* **22**, 617–621 (2020).
2. A. Ganguli, A. Mostafa, J. Berger, M. Y. Aydin, F. Sun, S. A. Stewart de Ramirez, E. Valera, B. T. Cunningham, W. P. King, R. Bashir, Rapid isothermal amplification and portable detection system for SARS-CoV-2. *Proc. Natl. Acad. Sci. U.S.A.* **117**, 22727–22735 (2020).
3. C. Myhrvold, C. A. Freije, J. S. Gootenberg, O. O. Abudayyeh, H. C. Metsky, A. F. Durbin, M. J. Kellner, A. L. Tan, L. M. Paul, L. A. Parham, K. F. Garcia, K. G. Barnes, B. Chak, A. Mondini, M. L. Nogueira, S. Isern, S. F. Michael, I. Lorenzana, N. L. Yozwiak, B. L. MacInnis, I. Bosch, L. Gehrke, F. Zhang, P. C. Sabeti, Field-deployable viral diagnostics using CRISPR-Cas13. *Science* **360**, 444–448 (2018).
4. I. Arevalo-Rodriguez, D. Buitrago-Garcia, D. Simancas-Racines, P. Zambrano-Achig, R. Del Campo, A. Ciapponi, O. Sued, L. Martinez-García, A. W. Rutjes, N. Low, P. M. Bossuyt, J. A. Perez-Molina, J. Zamora, False-negative results of initial RT-PCR assays for COVID-19: A systematic review. *PLOS ONE* **15**, e0242958 (2020).
5. F. Amanat, D. Stadlbauer, S. Strohmeier, T. H. O. Nguyen, V. Chromikova, M. McMahon, K. Jiang, G. A. Arunkumar, D. Jurczyszak, J. Polanco, M. Bermudez-Gonzalez, G. Kleiner, T. Aydillo, L. Miorin, D. S. Fierer, L. A. Lugo, E. M. Kojic, J. Stoever, S. T. H. Liu, C. Cunningham-Rundles, P. L. Felgner, T. Moran, A. García-Sastre, D. Caplivski, A. C. Cheng, K. Kedzierska, O. Vapalahti, J. M. Hepojoki, V. Simon, F. Krammer, A serological assay to detect SARS-CoV-2 seroconversion in humans. *Nat. Med.* **26**, 1033–1036 (2020).
6. C. Sheridan, Fast, portable tests come online to curb coronavirus pandemic. *Nat. Biotechnol.* **38**, 515–518 (2020).
7. R. Wölfel, V. M. Corman, W. Guggemos, M. Seilmaier, S. Zange, M. A. Müller, D. Niemeyer, T. C. Jones, P. Vollmar, C. Rothe, M. Hoelscher, T. Bleicker, S. Brünink, J. Schneider, R. Ehmann, K. Zwirglmaier, C. Drosten, C. Wendtner, Virological assessment of hospitalized patients with COVID-2019. *Nature* **581**, 465–469 (2020).
8. R. F. Service, Coronavirus antigen tests: Quick and cheap, but too often wrong? *Science* (2020).
9. R. Weissleder, H. Lee, J. Ko, M. J. Pittet, COVID-19 diagnostics in context. *Sci. Transl. Med.* **12**, eabc1931 (2020).
10. G. M. Joynt, W. K. Wu, Understanding COVID-19: What does viral RNA load really mean? *Lancet Infect. Dis.* **3099**, 19–20 (2020).
11. N. Cook, D. O. Cliver, Viruses: Detection, in *Encyclopedia of Food Microbiology* (Elsevier, 2014), vol. 3, pp. 727–731.
12. S. Khanal, P. Ghimire, A. Dhamoon, The repertoire of adenovirus in human disease: The innocuous to the deadly. *Biomedicine* **6**, 30 (2018).
13. M. R. Dunn, R. M. Jimenez, J. C. Chaput, Analysis of aptamer discovery and technology. *Nat. Rev. Chem.* **1**, 0076 (2017).
14. Z. Shen, Z. Wu, D. Chang, W. Zhang, K. Tram, C. Lee, P. Kim, B. J. Salena, Y. Li, A catalytic DNA activated by a specific strain of bacterial pathogen. *Angew. Chem. Int. Ed.* **55**, 2431–2434 (2016).
15. M. A. Page, J. L. Shisler, B. J. Mariñas, Kinetics of adenovirus type 2 inactivation with free chlorine. *Water Res.* **43**, 2916–2926 (2009).
16. K. Sefah, D. Shangguan, X. Xiong, M. B. O'Donoghue, W. Tan, Development of DNA aptamers using Cell-SELEX. *Nat. Protoc.* **5**, 1169–1185 (2010).
17. N. Kacherovsky, I. I. Cardle, E. L. Cheng, J. L. Yu, M. L. Baldwin, S. J. Salipante, M. C. Jensen, S. H. Pun, Traceless aptamer-mediated isolation of CD8+ T cells for chimeric antigen receptor T-cell therapy. *Nat. Biomed. Eng.* **3**, 783–795 (2019).
18. Q. Pan, F. Luo, M. Liu, X. L. Zhang, Oligonucleotide aptamers: Promising and powerful diagnostic and therapeutic tools for infectious diseases. *J. Infect.* **77**, 83–98 (2018).
19. C. L. A. Hamula, H. Peng, Z. Wang, G. J. Tyrrell, X.-F. Li, X. C. Le, An improved SELEX technique for selection of DNA aptamers binding to M-type 11 of Streptococcus pyogenes. *Methods* **97**, 51–57 (2016).
20. A. M. Gall, J. L. Shisler, B. J. Mariñas, Analysis of the viral replication cycle of adenovirus serotype 2 after inactivation by free chlorine. *Environ. Sci. Technol.* **49**, 4584–4590 (2015).

21. B. Vazquez-Bravo, K. Gonçalves, J. L. Shisler, B. J. Mariñas, Adenovirus replication cycle disruption from exposure to polychromatic ultraviolet irradiation. *Environ. Sci. Technol.* **52**, 3652–3659 (2018).
22. V. A. Avanzato, M. J. Matson, S. N. Seifert, R. Pryce, B. N. Williamson, S. L. Anzick, K. Barbian, S. D. Judson, E. R. Fischer, C. Martens, T. A. Bowden, E. de Wit, F. X. Riedo, V. J. Munster, Case study: Prolonged infectious SARS-CoV-2 shedding from an asymptomatic immunocompromised individual with cancer. *Cell* **183**, 1901–1912.e9 (2020).
23. Z. Luo, L. He, J. Wang, X. Fang, L. Zhang, Developing a combined strategy for monitoring the progress of aptamer selection. *Analyst* **142**, 3136–3139 (2017).
24. K. K. Alam, J. L. Chang, D. H. Burke, FASTAptamer: A bioinformatic toolkit for high-throughput sequence analysis of combinatorial selections. *Mol. Ther. Nucleic Acids* **4**, e230 (2015).
25. M. R. Gotrik, T. A. Feagin, A. T. Csordas, M. A. Nakamoto, H. T. Soh, Advancements in aptamer discovery technologies. *Acc. Chem. Res.* **49**, 1903–1910 (2016).
26. C. Bai, Z. Lu, H. Jiang, Z. Yang, X. Liu, H. Ding, H. Li, J. Dong, A. Huang, T. Fang, Y. Jiang, L. Zhu, X. Lou, S. Li, N. Shao, Aptamer selection and application in multivalent binding-based electrical impedance detection of inactivated H1N1 virus. *Biosens. Bioelectron.* **110**, 162–167 (2018).
27. T. Lu, Q. Ma, W. Yan, Y. Wang, Y. Zhang, L. Zhao, H. Chen, Selection of an aptamer against Muscovy duck parvovirus for highly sensitive rapid visual detection by label-free aptasensor. *Talanta* **176**, 214–220 (2018).
28. B. I. Escudero-Abarca, S. H. Suh, M. D. Moore, H. P. Dwivedi, L. A. Jaykus, Selection, characterization and application of nucleic acid aptamers for the capture and detection of human norovirus strains. *PLOS ONE* **9**, e106805 (2014).
29. T. R. Damase, T. A. Miura, C. E. Parent, P. B. Allen, Application of the open qPCR instrument for the in vitro selection of DNA aptamers against epidermal growth factor receptor and Drosophila C virus. *ACS Comb. Sci.* **20**, 45–54 (2018).
30. J. Hu, J. Kim, C. J. Easley, Quantifying aptamer–protein binding via thermofluorimetric analysis. *Anal. Methods* **7**, 7358–7362 (2015).
31. G. Pérez-Mitta, A. G. Albesa, C. Trautmann, M. E. Toimil-Molares, O. Azzaroni, Bioinspired integrated nanosystems based on solid-state nanopores: "Iontronic" transduction of biological, chemical and physical stimuli. *Chem. Sci.* **8**, 890–913 (2017).
32. U. F. Keyser, Enhancing nanopore sensing with DNA nanotechnology. *Nat. Nanotechnol.* **11**, 106–108 (2016).
33. A. Arima, I. H. Harlisa, T. Yoshida, M. Tsutsui, M. Tanaka, K. Yokota, W. Tonomura, J. Yasuda, M. Taniguchi, T. Washio, M. Okochi, T. Kawai, Identifying single viruses using biorecognition solid-state nanopores. *J. Am. Chem. Soc.* **140**, 16834–16841 (2018).
34. Z. Zhu, D. Wang, Y. Tian, L. Jiang, Ion/molecule transportation in nanopores and nanochannels: From critical principles to diverse functions. *J. Am. Chem. Soc.* **141**, 8658–8669 (2019).
35. Z. Sun, T. Liao, Y. Zhang, J. Shu, H. Zhang, G.-J. Zhang, Biomimetic nanochannels based biosensor for ultrasensitive and label-free detection of nucleic acids. *Biosens. Bioelectron.* **86**, 194–201 (2016).
36. T. Liao, X. Li, Q. Tong, K. Zou, H. Zhang, L. Tang, Z. Sun, G. J. Zhang, Ultrasensitive detection of microRNAs with morpholino-functionalized nanochannel biosensor. *Anal. Chem.* **89**, 5511–5518 (2017).
37. L. Mayne, C.-Y. Lin, S. D. R. Christie, Z. S. Siwy, M. Platt, The design and characterization of multifunctional aptamer nanopore sensors. *ACS Nano* **12**, 4844–4852 (2018).
38. P. Y. Apel, I. V. Blonskaya, S. N. Dmitriev, O. L. Orelovitch, A. Presz, B. A. Sartowska, Fabrication of nanopores in polymer foils with surfactant-controlled longitudinal profiles. *Nanotechnology* **18**, 305302 (2007).
39. G. Pérez-Mitta, A. S. Peinetti, M. L. Cortez, M. E. Toimil-Molares, C. Trautmann, O. Azzaroni, Highly sensitive biosensing with solid-state nanopores displaying enzymatically reconfigurable rectification properties. *Nano Lett.* **18**, 3303–3310 (2018).
40. X. Hou, W. Guo, F. Xia, F.-Q. Nie, H. Dong, Y. Tian, L. Wen, L. Wang, L. Cao, Y. Yang, J. Xue, Y. Song, Y. Wang, D. Liu, L. Jiang, A biomimetic potassium responsive nanochannel: G-quadruplex DNA conformational switching in a synthetic nanopore. *J. Am. Chem. Soc.* **131**, 7800–7805 (2009).
41. Y. Guo, J. Tisoncik, S. McReynolds, M. Farzan, B. S. Prabhakar, T. Gallagher, L. Rong, M. Caffrey, Identification of a new region of SARS-CoV S protein critical for viral entry. *J. Mol. Biol.* **394**, 600–605 (2009).
42. Q. Cui, H. Cheng, R. Xiong, G. Zhang, R. Du, M. Anantpadma, R. Davey, L. Rong, Identification of diaryl-quinoline compounds as entry inhibitors of Ebola virus. *Viruses* **10**, 678 (2018).
43. X. Ou, Y. Liu, X. Lei, P. Li, D. Mi, L. Ren, L. Guo, R. Guo, T. Chen, J. Hu, Z. Xiang, Z. Mu, X. Chen, J. Chen, K. Hu, Q. Jin, J. Wang, Z. Qian, Characterization of spike glycoprotein of SARS-CoV-2 on virus entry and its immune cross-reactivity with SARS-CoV. *Nat. Commun.* **11**, 1620 (2020).
44. J. P. Broughton, W. Deng, C. L. Fasching, J. Singh, Y. Charles, J. S. Chen, M. Biosciences, S. S. Francisco, S. Francisco, S. Francisco, A protocol for rapid detection of SARS-CoV-2 using CRISPR: SARS-CoV-2 DETECTR (Mammoth Biosciences, 2020), pp. 1–9.
45. V. L. Dao Thi, K. Herbst, K. Boerner, M. Meurer, L. P. Kremer, D. Kirrmaier, A. Freistaedter, D. Papagiannidis, C. Galmozzi, M. L. Stanifer, S. Boulant, S. Klein, P. Chlanda, D. Khalid, I. B. Miranda, P. Schnitzler, H.-G. Kräusslich, M. Knop, S. Anders, A colorimetric RT-LAMP assay and LAMP-sequencing for detecting SARS-CoV-2 RNA in clinical samples. *Sci. Transl. Med.* **12**, eabc7075 (2020).
46. P. S. Kwon, S. Ren, S. Kwon, M. E. Kizer, L. Kuo, M. Xie, D. Zhu, F. Zhou, F. Zhang, D. Kim, K. Fraser, L. D. Kramer, N. C. Seeman, J. S. Dordick, R. J. Linhardt, J. Chao, X. Wang, Designer DNA architecture offers precise and multivalent spatial pattern-recognition for viral sensing and inhibition. *Nat. Chem.* **12**, 26–35 (2020).
47. M. Tagliazucchi, O. Azzaroni, I. Szleifer, Responsive polymers end-tethered in solid-state nanochannels: When nanoconfinement really matters. *J. Am. Chem. Soc.* **132**, 12404–12411 (2010).
48. F. M. Gilles, M. Tagliazucchi, O. Azzaroni, I. Szleifer, Ionic conductance of polyelectrolyte-modified nanochannels: Nanoconfinement effects on the coupled protonation equilibria of polyprotic brushes. *J. Phys. Chem. C* **120**, 4789–4798 (2016).
49. Y. Song, J. Song, X. Wei, M. Huang, M. Sun, L. Zhu, B. Lin, H. Shen, Z. Zhu, C. Yang, Discovery of aptamers targeting the receptor-binding domain of the SARS-CoV-2 spike glycoprotein. *Anal. Chem.* **92**, 9895–9900 (2020).
50. A. Schmitz, A. Weber, M. Bayin, S. Breuers, V. Fieberg, M. Famulok, G. Mayer, A SARS-CoV-2 spike binding DNA aptamer that inhibits pseudovirus infection by an RBD-independent mechanism*. *Angew. Chem. Int. Ed.* **60**, 10279–10285 (2021).
51. M. Sun, S. Liu, X. Wei, S. Wan, M. Huang, T. Song, Y. Lu, X. Weng, Z. Lin, H. Chen, Y. Song, C. Yang, Aptamer blocking strategy inhibits SARS-CoV-2 virus infection. *Angew. Chem. Int. Ed.* **60**, 10266–10272 (2021).
52. E. W. Rice, R. B. Baird, A. D. Eaton, Eds., *Standard Methods for the Examination of Water and Wastewater* (American Public Health Association, ed. 23, 2017).
53. J. R. Bolton, K. G. Linden, Standardization of methods for fluence (UV Dose) determination in bench-scale UV experiments. *J. Environ. Eng.* **129**, 209–215 (2003).
54. T. L. Cromeans, X. Lu, D. D. Erdman, C. D. Humphrey, V. R. Hill, Development of plaque assays for adenoviruses 40 and 41. *J. Virol. Methods* **151**, 140–145 (2008).
55. A. M. Gall, J. L. Shisler, B. J. Mariñas, Inactivation kinetics and replication cycle inhibition of adenovirus by monochloramine. *Environ. Sci. Technol. Lett.* **49**, 4584–4590 (2016).
56. L. Zhang, X. Fang, X. Liu, H. Ou, H. Zhang, J. Wang, Q. Li, H. Cheng, W. Zhang, Z. Luo, Discovery of sandwich type COVID-19 nucleocapsid protein DNA aptamers. *Chem. Commun.* **56**, 10235–10238 (2020).

Acknowledgments: We thank K. Goncalves for preparing the initial adenovirus samples, the Urbana and Champaign Sanitary District (IL, USA) for providing the wastewater samples, and the Panyodoli Secondary School in Kiryandongo District (Uganda) for providing the borehole water samples. T. Gallagher at Loyola University supplied the 229E coronavirus , Huh-7 cell line, the SARS-CoV-2 S-protein plasmid, and the SARS-CoV-1 S-protein plasmid. HTS was performed by the DNA Services Lab of the Roy J. Carver Biotechnology Center at UIUC, and we thank A. Hernandez and C. Wright for help in advising for the DNA library preparation and for performing the Illumina sequencing. **Funding:** This work was supported by a RAPID grant from the National Science Foundation (CBET 20-29215) and a seed grant from the Institute for Sustainability, Energy, and Environment at University of Illinois at Urbana-Champaign and Illinois-JITRI Institute (JITRI 23965). A.S.P. thanks the PEW Latin American Fellowship for financial support. The irradiated PET foils are part of the experiment UMAT, which was performed at the beam line X0 at the GSI Helmholtzzentrum für Schwerionenforschung (Darmstadt, Germany) in the frame of FAIR Phase-0. O.A. acknowledges financial support from CONICET (PIP0370) and ANPCyT (PICT-2016-1680 and PICT-2017-1523). **Author contributions:** A.S.P., B.M., and Y.L. conceptualized the study. A.S.P., O.A., B.M., L.R., and Y.L. designed methodology. A.S.P. and R.J.L. performed and analyzed the experiments related with aptamer SELEX and nanopore measurements. A.S.P., Y.W., Y.M., and G.T.P. performed binding affinity assay experiments. W.C. and L.C. prepared the virus and pseudovirus samples and performed microbiology experiments. O.A., M.E.T.-M., and C.T. synthesized the solid-state nanopore and designed the nanopore measurement setup. Y.L. was responsible for project supervision, direction, and resource acquisition. A.S.P., R.J.L., and Y.L. wrote the manuscript, and all authors edited and reviewed it. **Competing interests:** A.S.P., O.A., and Y.L. are inventors on a patent application filed by University of Illinois at Urbana-Champaign (no. PCT/US2021/033245, filed on 19 May 2021). O.A. is a consultant and scientific advisor for Gisens Biotech. Y.L. is a cofounder and board member of ANDalyze Inc. and GlucoSentient Inc. The authors declare no other competing interests. **Data and materials availability:** All data needed to evaluate the conclusions in the paper are present in the paper and/or the Supplementary Materials. The aptamer can be provided by the Lu group, and the SARS-CoV-2 pseudovirus can be provided by the Rong group pending scientific review and a completed material transfer agreement. Requests for the aptamer should be submitted to Y.L. (yi-lu@illinois.edu), and requests for the SARS-CoV-2 pseudovirus should be submitted to L.R. (lijun@uic.edu).

Submitted 2 March 2021
Accepted 2 August 2021
Published 22 September 2021
10.1126/sciadv.abh2848

Citation: A. S. Peinetti, R. J. Lake, W. Cong, L. Cooper, Y. Wu, Y. Ma, G. T. Pawel, M. E. Toimil-Molares, C. Trautmann, L. Rong, B. Mariñas, O. Azzaroni, Y. Lu, Direct detection of human adenovirus or SARS-CoV-2 with ability to inform infectivity using DNA aptamer-nanopore sensors. *Sci. Adv.* **7**, eabh2848 (2021).

ScienceAdvances

Direct detection of human adenovirus or SARS-CoV-2 with ability to inform infectivity using DNA aptamer-nanopore sensors

Ana S. PeinettiRyan J. LakeWen CongLaura CooperYuting WuYuan MaGregory T. PawelMaría Eugenia Toimil-MolaresChristina TrautmannLijun RongBenito MariñasOmar AzzaroniYi Lu

Sci. Adv., 7 (39), eabh2848. • DOI: 10.1126/sciadv.abh2848

Science Advances (ISSN) is published by the American Association for the Advancement of Science. 1200 New York Avenue NW, Washington, DC 20005. The title *Science Advances* is a registered trademark of AAAS.